RSC Advances

ROYAL SOCIETY OF CHEMISTRY

www.rsc.org/advances

Journal Name

COMMUNICATION

Mesoporous Silica Nanospheres Supported Platinum Nanoparticles (Pt@MSN): One-pot Synthesis and Catalytic Hydrogen Generation

Received 00th January 20xx,
Accepted 00th January 20xx

DOI: 10.1039/x0xx00000x

www.rsc.org/

Maria Irum,[a] Muhammad Zaheer,[a*] Martin Friedrich,[b] and Rhett Kempe,[b]

One-pot synthesis of mesoporous silica nanospheres (MSN) supported platinum nanoparticles (NPs) as catalysts for hydrogen generation from alkaline sodium borohydride is reported. Size of NPs can somehow be tuned by the pore size of the MSN provided the metal loading isn't high. The catalysts provided a turnover frequency (TOF) of 11274h^{-1} with a hydrogen generation rate (HGR) of 19 L.min^{-1}g^{-1} Pt.

With the depletion of fossil fuels, and increasing environmental issues, energy demands across the globe are turning towards sustainable energy sources.[1,2] Thus hydrogen has been found a promising candidate in this perspective in terms of its use in fuel cells for the generation of clean and renewable energy.[3,4] The mightier challenge is still the cheap and safe storage of hydrogen gas and for the past few decades chemical hydrogen storage in various liquids and solids has been intensively investigated[5–9]. Chemical hydrides[10,11] such as sodium borohydride ($NaBH_4$; SBH), lithium borohydride ($LiBH_4$), and sodium aluminiumhydride ($NaAlH_4$), in this regard, have received much attention as promising hydrogen storage materials in view of being economic and high energy content which could meet 9% global energy demand as declared by U.S. Department of Energy (DOE) by 2015.[12] Among all the chemical hydrides, SBH is found to be more promising because of its high hydrogen content (10.8 wt.%), stability in basic medium and potential reversible hydrogen storage.[13,14] However, it can be conveniently hydrolyzed using metal catalysts.[15] Standard enthalpy change for hydrolysis[16] reaction shows that reaction is highly exothermic and spontaneously hydrolyzes to H_2 and water soluble $NaBO_2$ as shown in equation below:

$$NaBH_4 + 2H_2O \longrightarrow NaBO_2 + 4H_2 \qquad \Delta H = -217 KJ/mol$$

[a] Department of Chemistry, SBA School of Science and Engineering (SBASSE), Lahore University of Management Sciences (LUMS), Lahore 54792 Pakistan.
[b] Anorganische Chemie II, Universitaet Bayreuth, Bayreuth 95447 Germany.
*Corresponding author email: muhammad.zaheer@lums.edu.pk
Phone: +92-423-5608465, Fax:
† Footnotes relating to the title and/or authors should appear here.
Electronic Supplementary Information (ESI) available: [details of any supplementary information available should be included here]. See DOI: 10.1039/x0xx00000x

Due to their high activity for catalytic hydrolysis of SBH, upported Pt catalysts[17–26] has been extensively investigated. The ideal catalyst should however provide high hydrogen generation rate (HGR) at ambient conditions and should be robust enough to be collected and reused.

Since their discovery in 1992[27], mesoporous silica (MCM-41) has been synthesized in a variety of morphologies such as nanospheres (MSN) prepared via a modified Stoeber method.[28] Due to their colloidal size regime (<1000 nm), high surface area, ordered pore structure and narrow pore size distribution (2-10 nm), MSN find applications as MRI contrast agent[29], drug delivery[30], biosensing[31] and catalysis[32]. Metal nanoparticles (NPs) supported over mesoporous silica is perhaps among the most widely used heterogeneous catalysts used for a variety of catalytic transformations ranging from organic synthesis to renewable energy production and storage.[33] Such catalysts are normally synthesized in a two-step process: first step being the synthesis of mesoporous silica followed by the incorporation of metal NPs via impregnation, chemical vapour deposition (CVD) and others.[34] Such methods don't give control over the morphology and size of the NPs formed and possible leaching of the loosely bound metal NPs is more likely. A one-pot process involving the both the synthesis of mesoporous silica and generation of metal NPs is attractive in the sense that would allow the cavity confined growth of monosized particles with an expectation of low metal leaching and better reusability. For instance, Wan *et al* has recently reported a one-pot synthesis of palladium (Pd) NPs within the channels of MCM-41 and has shown that the catalysts is reusable multiple times.[35]

Here we report one-pot synthesis of highly active, cavity confided and monosized platinum (Pt) NPs within the channels of MSNs (catalysts are thus named Pt@MSN). The catalysts provided a very high TOF (11274h^{-1}) for the hydrolysis of SBH. Synthesis of Pt@MSN materials is summarized in scheme 1. Spherical micelle (II in scheme 1) of surfactant Cetyltrimethylammonium bromide (CTAB, I in scheme 1) assembles in hexagonal array (IV in scheme 1) around which

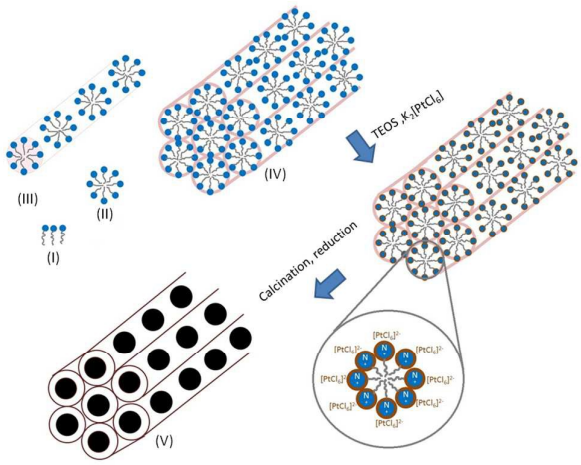

Scheme 1. One-pot synthesis of Pt@MSN materials. Steps I-IV explain the micellization and assembly of CTAB; Final material Pt@MSN (V) with cavity confined Pt NPs.

the SiO_2 starts growing from the hydrolysis of tetraethylorthosilicate (TEOS). Any metal –ate complex added at this moment should coordinate with positive nitrogen of CTAB which would be converted to elemental metal after calcinations and reduction steps.

FT-IR spectrum of the materials (figure 1a) showed characteristic bands of Si-O linkages at 1053 and 805 cm^{-1} while a sharp peak at 2923 cm^{-1} was assigned to the stretching vibration of -OH groups in the sample before calcination. After calcination only two peaks at 1064 cm^{-1} (Si-O-Si) and 805 cm^{-1} (surface silanols, Si-O-H) were identified.[36]

The presence of elemental platinum was confirmed by powder XRD analysis of the materials. All of the synthesized materials, show (figure 1b) a broad band at 21°(2θ) characteristic of amorphous silica and the most intense (111) reflection of cubic platinum at 39.9°(2θ). The breadth of (111) reflection increases with the loading of metal due to an increase in the

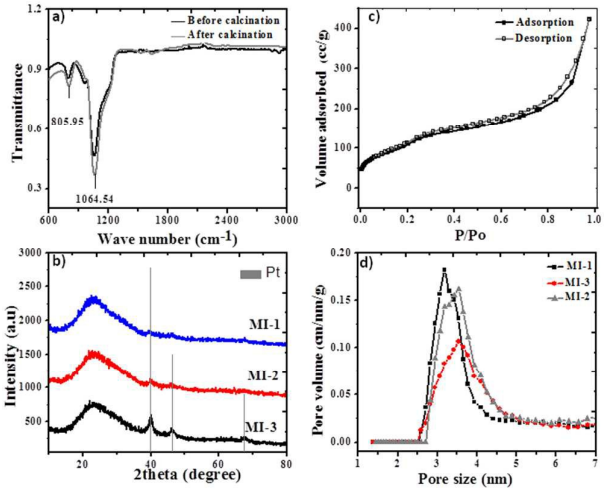

Figure 1. a) FT-IR of a representative sample (MI-1); b) Powder XRD patterns; c) nitrogen adsorption-desorption isotherm (MI-1) and d) pore size distribution.

size of platinum NPs. Complete reflection pattern of platinum however was identified only for MI-3 (9.6 wt% Pt) at 39.99°, 46.50° and 67.66° *(JCPDS 00-001-1194)* corresponding to 111, 220 and 222 planes respectively. Average crystallite size for this material with the highest metal loading was calculated to be 14.4 nm (calculated using Sherrer equation).

Pt@MSN catalysts showed type-IV nitrogen adsorption-desorption isotherms as shown in a representative isotherm shown in figure 1c. Hysteresis in the isotherm along with the closure of desorption loop at P/P_0 is typical of mesoporous materials[37]. As compared to MCM-41 without metal loading (entry 1, table 1) surface area of the materials loaded with metal was found fairly wt.%) (b) MI-2 (4.8 wt.%) (c) MI-3 (9.6 wt.%) small (entries 2-4). It can be justified that in situ encapsulation of metal particles inside the pores has led to considerable decrease in specific surface area. This reduction in surface area is much pronounced for 2.4 and 4.8 wt.% metal content (entry 2 and 3) which suggests the smaller sized metal NPs contained by the pores whereas in case of the material with 9.6 wt.% metal (entry 4), specific surface area is higher owing to the large sized particles sitting on the surface instead of within the pores. The pore size (figure 1d) slightly increased with increasing metal content whereas pore volume decreased as compared to MCM-41.[35]

The microstructure of the as synthesized catalysts was analyzed by TEM (figure 2). Silica particles adopted oval shape morphology (a-b) with a size regime of (~200 nm). Typical hexagonal channels of MCM-41 with or without enclosed metal nanoparticles (NPs) can be seen in images d-f of figure 2. NPs mainly remained within the channels and small sized (see figure 2d) when the loading of the metal was low (2.4 wt%). However not all the pores were occupied by the NPs. As the metal loading was increased to 4.8 wt%, the population density of filled pores also increased (see figure 2e). The size of the NPs, occupying the channels remained small however, those NPs sitting on the surface increased in size to much extent (figure 2e). With a further increase in metal loading (9.6 wt%), the size of surface NPs particles was further increased (figure 2f). It can be concluded at this point that size of the metal NPs can somehow be tuned by the size of pores contained by the materials provided the loading of metal is low. In this way monosized particles with the sizes in the dimension of the pores (3 nm) can be generated. With the increase in metal loading, almost all the pores get occupied and additional metal sits over the surface as NPs whose size increases with the increase in metal loading. These claims are supported by nitrogen adsorption studies on the synthesized materials.

Table1. Surface area, pore size and pore volume of synthesized materials

Entry	Material	Surface area ($m^2.g^{-1}$)	Pore size (nm)	Pore volume ($cc.g^{-1}$)
1	MCM-41	955	3.1	0.93
2	MI-1 (2.4 wt.%)	361	3.2	0.554
3	MI-2 (4.8 wt.%)	340	3.5	0.790
4	MI-3 (9.6 wt.%)	405	3.5	0.731

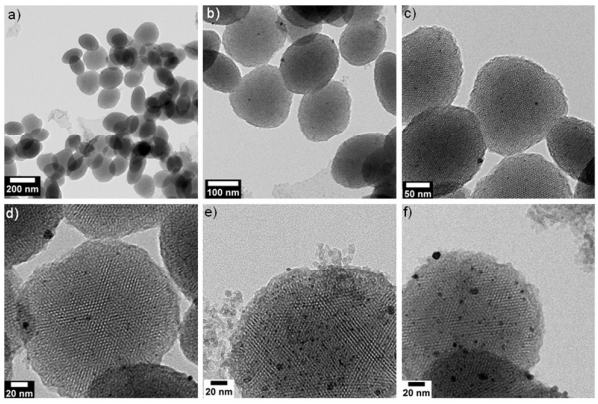

Figure 2. TEM micrographs of Pt@MSN materials. a-d) MI-1 (2.4 wt.% Pt); e) MI-2 (4.8 wt.% Pt); f) MI-3 (9.6 wt.% Pt)

Effect of various parameters such as metal loading, catalyst amount, temperature, $NaBH_4$ concentration and NaOH concentration on the catalytic activity of Pt@MSN materials were investigated (figure 3). As expected HGR ($L.min^{-1}g^{-1}$ Pt) increased with an increase in metal loading (figure 3a) from 2.4%(MI-1, 0.44) to 4.8% (MI-2, 0.47) and 9.6%(MI-3, 0.87). One would expect such behaviour owing to increase in number of active sites exposed on surface. Turnover frequencies (TOF) are provided in tables S1-S5.

HGR with respect to change in concentration of sodium borohydride (figure S1a) was calculated by increasing concentration from 1.25-10 wt%. Highest HGR (0.872) at 25°C was calculated for 5wt% solution. Increasing solution concentration above 5wt% resulted in lower HGR most probably due to increase in solution viscosity which would have afforded mass transport constraints.[14]

Aqueous solution of $NaBH_4$ undergoes self-hydrolysis even at ambient temperature which can be inhibited by the addition of base as stabilizer.[13] Figure S1b Illustrates volume of hydrogen gas evolved as a function of concentration of NaOH. An almost constant HGR was observed at all base concentration which leads us to the conclusion that hydrolysis of $NABH_4$ is zero order with respect to base concentration. Effect of metal loading, SBH concentration, base concentration, temperature and catalyst dose on TONs and TOFs are given in supporting information (tables S1-S5)

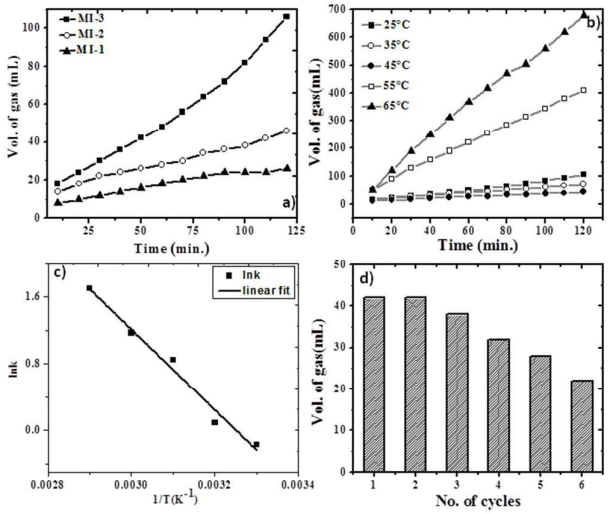

Figure 3. Catalytic hydrolysis of $NaBH_4$ using at Pt@MSN catalyst (MI-3). A) effect of metal loading on HGR; b) effect of temperature; c) Arrhenius plot; d) Recycling test.

Figure 3b compares the volume of hydrogen gas evolved as a function of temperature varying from 25-65°C. As the temperature is increased volume of evolved hydrogen also increases gradually,[16] the highest HGR was found at 80°C (19.1 $Lmin^{-1}g^{-1}$ Pt). If we compare the activity of our catalysts with other Pt-based catalysts, we obtained a very good TOF (11274 h^{-1}) as compared to other Pt and noble metals based solid catalysts reported[38] (table S6) Furthermore, as compared to the literature, relatively lower activation energy (40.1 $KJmol^{-1}$) for the hydrolysis reaction was measured from Arrhenius plot (figure 3c).

Recyclability and reusability of catalyst is a crucial parameter in heterogeneous catalysis. Thus in order to make process viable in practical HG applications catalytic activity was measured up to five successive runs. Results (see figure 3d) showed that catalyst sustained its activity up till three successive runs after which it lost its activity. Powder XRD analysis of the used catalyst (MI-3, Figure S2) showed an increase in the size of Pt NPs (from 14 nm to 29 nm) as calculated by Scherrer formula. FT-IR analyses of the used catalyst (Figure S3) were also done in order to check whether the cause of the reduction in activity was pore blockage by the metaborate[39]. Absorption bands at 1600-1200 cm^{-1} may be attributed to stretching vibrations of B-O bonds of sodium metaborate.[40] Thus decrease in the activity could be due to increase in the particle size as well as pore blockage by metaborates. Inductively coupled plasma optical emission spectroscopy (ICP-OES) analysis of the fresh and used catalyst was also carried out and no reduction in metal content was observed. The reduction in the volume of evolved hydrogen gas was worse in the case of MI-3 (with 9.6 wt% Pt, figure S1d) as compared to the one with a low metal loading (MI-1, 2.4 wt% Pt, figure 3d).

Conclusions

One-pot synthesis of Pt NPs within the channels of mesoporous silica nanospheres afforded materials in which metal NPs somehow remain small in size (decided by the size of the channels in which they reside). This cavity confinement of NPs and thus their monodispersity depends upon the metal loading-the lower the better. High HGR from SBH hydrolysis was observed with high TOFs. The volume of evolved hydrogen decreased gradually with increase in number of recycles most probably not due to the leaching of the metal but because of the blockage of the pore (and thus active sites) with metaborate.

Notes and references

1 N. Armaroli and V. Balzani, *Angew. Chem., Int. Ed.*, 2007, **46**, 52–66.
2 S. Chu and A. Majumdar, *Nature*, 2012, **488**, 294–303.
3 L. Schlapbach and A. Züttel, *Nature*, 2001, **414**, 353–358.
4 U. Eberle, M. Felderhoff and F. Schüth, *Angew. Chem. Int. Ed. Engl.*, 2009, **48**, 6608–30.
5 L. J. Murray, M. Dincă and J. R. Long, *Chem. Soc. Rev.*, 2009, **38**, 1294–314.
6 R. H. Crabtree, *Energy Environ. Sci.*, 2008, **1**, 134.
7 A. Boddien, F. Gärtner, C. Federsel, P. Sponholz, D. Mellmann, R. Jackstell, H. Junge and M. Beller, *Angew. Chem. Int. Ed. Engl.*, 2011, **50**, 6411–4.
8 G. Papp, J. Csorba, G. Laurenczy and F. Joó, *Angew. Chemie*, 2011, **123**, 10617–10619.
9 E. Environ, M. Yadav and Q. Xu, 2012, 9698–9725.
10 S.-I. Orimo, Y. Nakamori, J. R. Eliseo, A. Züttel and C. M. Jensen, *Chem. Rev.*, 2007, **107**, 4111–32.
11 B. Sakintuna, F. Lamaridarkrim and M. Hirscher, *Int. J. Hydrogen Energy*, 2007, **32**, 1121–1140.
12 C. H. Liu, B. H. Chen, C. L. Hsueh, J. R. Ku, M. S. Jeng and F. Tsau, *Int. J. Hydrogen Energy*, 2009, **34**, 2153–2163.
13 U. B. Demirci, *Int. J. Hydrogen Energy*, 2015, **40**, 2673–2691.
14 Y. Kojima and T. Haga, *Int. J. Hydrogen Energy*, 2003, **28**, 989–993.
15 P. Brack, S. E. Dann and K. G. U. Wijayantha, *Energy Sci. Eng.*, 2015, **3**, 174–188.
16 Y. Kojima, K. Suzuki, K. Fukumoto, M. Sasaki, T. Yamamoto, Y. Kawai and H. Hayashi, *Int. J. Hydrogen Energy*, 2002, **27**, 1029–1034.
17 T.-F. Hung, H.-C. Kuo, C.-W. Tsai, H. M. Chen, R.-S. Liu, B.-J. Weng and J.-F. Lee, *J. Mater. Chem.*, 2011, **21**, 11754.
18 C. Salameh, A. Bruma, S. Malo, U. B. Demirci, P. Miele and S. Bernard, *RSC Adv.*, 2015, **5**, 58943–58951.
19 Z. Liu, B. Guo, S. H. Chan, E. H. Tang and L. Hong, *J. Power Sources*, 2008, **176**, 306–311.
20 Y. Bai, C. Wu, F. Wu and B. Yi, *Mater. Lett.*, 2006, **60**, 2236–2239.
21 D. Xu, H. Wang, P. Dai and Q. Ye, *Open Catal. J.*, 2009, **2**, 92–95.
22 D. Xu, H. Zhang and W. Ye, *Catal. Commun.*, 2007, **8**, 1767–1771.
23 Y. Hu, Y. Wang, Z.-H. Lu, X. Chen and L. Xiong, *Appl. Surf. Sci.*, 2015, **341**, 185–189.
24 I. Boran, A. Erkan, S. Ozkar, S. Eroglu, *Int. J. energy Res.*, 2013, **37**, 443–448.
25 U. B. Demirci and F. Garin, *Int. J. Green Energy*, 2008, **5**, 148–156.
26 M. Sankir, L. Semiz, R. B. Serin and N. D. Sankir, *Int. J. Hydrogen Energy*, 2015, **40**, 8522–8529.
27 J. Kresge, CT, Leonowicz, ME, Roth, WJ, Vartuli, JC, Beck, *Nature*, 1992, **359**, 710–712.
28 S.-H. Wu, C.-Y. Mou and H.-P. Lin, *Chem. Soc. Rev.*, 2013, **42**, 3862.
29 K. M. L. Taylor, J. S. Kim, W. J. Rieter, H. An, W. Lin and W. Lin, *J. Am. Chem. Soc.*, 2008, **130**, 2154–+.
30 I. Slowing, J. Viveroescoto, C. Wu and V. Lin, *Adv. Drug Deliv. Rev.*, 2008, **60**, 1278–1288.
31 I. I. Slowing, B. G. Trewyn, S. Giri and V. S. Y. Lin, *Adv. Funct. Mater.*, 2007, **17**, 1225–1236.
32 D. J. Mihalcik and W. Lin, *Angew. Chemie - Int. Ed.*, 2008, **47**, 6229–6232.
33 R. Luque, A. M. Balu, J. M. Campelo, M. D. Gracia and E. Losada, *Catalytic applications of mesoporous silica- based materials in Catalysis (Eds)*, Royal Society of Chemistry, 2012, vol. 24.
34 J. a. Schwarz, C. Contescu and A. Contescu, *Chem. Rev.*, 1995, **95**, 477–510.
35 X.-J. Lin, A.-Z. Zhong, Y.-B. Sun, X. Zhang, W.-G. Song, R.-W. Lu, A.-M. Cao and L.-J. Wan, *Chem. Commun.*, 2015, **51**, 7482–7485.
36 Y. Gao, Q. Dong, S. Lan, Q. Cai, O. Simalou, S. Zhang, G. Gao, H. Chokto and A. Dong, *ACS Appl. Mater. Interfaces*, 2015, **7**, 10022–10033.
37 M. Zaheer, J. Hermannsdörfer, W. P. Kretschmer, G. Motz and R. Kempe, *ChemCatChem*, 2014, **6**, 91–95.
38 U. B. Demirci, O. Akdim, J. Andrieux, J. Hannauer, R. Chamoun and P. Miele, *Fuel Cells*, 2010, **10**, 335–350.
39 M. H. Loghmani and A. F. Shojaei, *Energy*, 2014, **68**, 152–159.
40 E. Mansour, J. *Mol. Struct*. 2012, **1014**, 1-6.

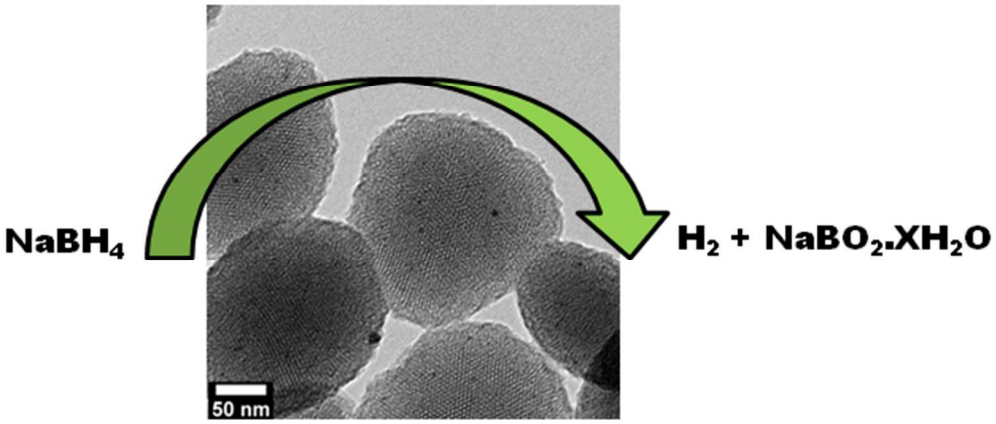

166x72mm (96 x 96 DPI)